Environmental Science Advances

ROYAL SOCIETY OF CHEMISTRY

PAPER

View Article Online
View Journal | View Issue

Cite this: *Environ. Sci.: Adv.*, 2025, **4**, 663

Synthesis of calcined LDHs materials decorated on ZnO nanorods: enhancing adsorption capacity and antibacterial activity†

T. V. M. Sreekanth,[a] Huu Phuc Dang,[b] Nguyen Quoc Thang,[c] Nguyen Van Cuong[c] and Nguyen Thi Mai Tho *[c]

In this study, ZnCo-layered double hydroxides (ZnCo-LDHs) were successfully synthesized *via* a co-precipitation method using zinc nitrate and cobalt nitrate in a 3 : 1 molar ratio on ZnO rods (ZnO/ZnCo-LDHs). Subsequent heat treatment of the ZnO/ZnCo-LDHs at 600 °C transformed them into $ZnCo_2O_4$ and ZnO, which were evenly distributed within the ZnO rods. The adsorption capacity of Reactive Blue 221 (RB221) using the ZnO/ZnCo-cLDHs composites reached 75.74 (mg g^{-1}) in 100 min under the following conditions: initial RB221 concentration of 80 ppm, pH 7, and a dose of 1.0 g L^{-1}. The mechanism of dye adsorption on the ZnO/ZnCo-cLDHs was determined by the "memory effect" of oxide and available vacant sites between interlayers of adsorption mixtures. The Langmuir adsorption isotherm was more efficient in explaining the adsorption of RB221 dye on ZnO/ZnCo-cLDHs than the Freundlich isotherm. Experimental data indicated that the second-order kinetic equation is a more suitable model for describing the adsorption process than the first-order kinetic equation. Furthermore, the ZnO/ZnCo-cLDHs composites demonstrated antibacterial properties, inhibiting the growth of *Escherichia coli*, *Staphylococcus aureus*, and *Salmonella typhimurium*.

Received 9th December 2024
Accepted 3rd February 2025

DOI: 10.1039/d4va00413b

rsc.li/esadvances

Environmental significance

Industrial production generates several items for consumption by humans yet simultaneously emits various harmful compounds that significantly impact the aquatic environment. This article enhances traditional adsorbent materials to augment their efficacy in treating textile wastewater, supplying clean water to people.

1. Introduction

Environmental contamination, specifically water pollution, is increasing in many countries. The volume of organic waste in wastewater due to industrial operations, such as coatings, paper production, tanning, food, and textiles, is considerable.[1–3] The introduction of these pollutants into water is currently eliciting significant concerns due to their harmful impact on human and animal health. To swiftly eliminate organic pollutants and supply clean water to people, new techniques must be developed and existing ones must be improved in addition to increasing the awareness for environmental preservation.[4,5] Multiple methods such as coagulation, ion exchange, membrane filtration and precipitation, and photocatalysis have been employed to remove effluents from textiles.[6–9] However, these techniques may be too costly and unfeasible for widespread implementation. Adsorption is an attractive option for minimizing the abovementioned disadvantages by effectively eliminating hazardous pollutants from water.[2,6,10]

Recently, there has been significant interest in the use of mixed-metal oxides derived from LDHs for adsorption.[11–13] These materials are attracting attention because of their cost-effectiveness, excellent chemical stability, relative safety, biological compatibility, and the ability to be easily synthesized with different metal compositions for specific application requirements.[14,15] The general formula for LDHs is $[M_{1-a}^{2+}M_a^{3+}(OH)_2]^{a+}[A^{n-}]_{a/n}\cdot mH_2O$, where A^{n-} is an interlayer anion, M^{2+} is a divalent metal cation, and M^{3+} is a trivalent metal cation.[13,14] LDHs are structural layers with interlayers of H_2O and flexible anions; therefore, they exhibit high ion-exchange capacity.[16] The LDHs are destroyed by the structure of layers, and mixed oxides (MMO) are formed when heated between 400 °C and 600 °C.[13,17] cLDHs possess greater surface areas and exhibit enhanced thermal and chemical stability in addition to a higher density of active sites compared to LDHs.[18]

[a]*School of Mechanical Engineering, Yeungnam University, Gyeongsansi, Gyeongsangbukdo, Republic of Korea*

[b]*Faculty of Fundamental Science, Industrial University of Ho Chi Minh City, Ho Chi Minh City, Vietnam*

[c]*Faculty of Chemical Engineering, Industrial University of Ho Chi Minh City, Ho Chi Minh City, Vietnam. E-mail: nguyenthimaitho@iuh.edu.vn*

† Electronic supplementary information (ESI) available. See DOI: https://doi.org/10.1039/d4va00413b

When MMO come into contact with anions in a water solution, one of their most significant properties is the "memory effect," which is a mechanism that rebuilds the LDHs structure.[11,12] In addition, cLDHs have been used as adsorbent materials because of their large specific surface area, efficient dispersion of active species, thermal stability, and porous characteristics.[19,20]

To enhance the effectiveness of pollutant removal using cLDHs, researchers have conducted studies on mixing cLDHs with other materials.[1,18,21] Numerous studies have shown that the surface properties and adsorption effectiveness of cLDHs are enhanced when combined with other materials, such as polymers, clay, semiconductors, and surfactants.[18] The surface performance and adsorption capacity can be significantly enhanced by combining cLDHs with carbon, which increases the surface area and enriches the oxidizing functional groups.[22–24] Many types of composite materials have been studied, including C@MgAl-cLDHs,[25] ZnO/MgAl-cLDHs,[17] cLDHs/MOF,[26] and GCN/cLDHs.[21] Additionally, cLDHs and composites are excellent choices for certain biological applications.[27] Electrostatic interactions between cationic cLDHs and negatively charged bacterial surfaces may suppress bacterial growth.[28,29] One-dimensional (1D) nanomaterials, known as nanorods, have a variety of uses and better chemical and physical characteristics than other structures.[6,30] ZnO nanorods is a non-toxic, extremely stable metal oxide with good adsorption ability for removing contaminants from water.[22,31] However, composites formed by combining cLDHs with ZnO nanorods have remained relatively unexplored.

This work effectively developed ZnO rods/ZnCo-cLDHs to increase the adsorption performance and surface characteristics of the composites. ZnO/ZnCo-LDHs were synthesized on ZnO rods using the hydrothermal and co-precipitation methods. The adsorption of RB221 on ZnO/ZnCo-cLDHs was tested under various equilibrium conditions. The underlying mechanism of RB221 adsorption on ZnO/ZnCo-cLDHs was investigated by analyzing the adsorption kinetics and isotherm patterns. The minimum inhibitory concentrations (MIC) of the bacterial strains were calculated, and the antibacterial properties of the composites were assessed.

2. Experimental

2.1 Synthesized ZnO rods

ZnO rods were synthesized using a simple thermal method.[32] 2.1 g of $Zn(NO_3)_2 \cdot 6H_2O$ (99%; Sigma-Aldrich) was dissolved in 50 mL of distilled water. The $Zn(NO_3)_2$ solution was stirred while slowly adding 4 M NH_4OH (25%; Xilong-China) solution until the pH reached 11. The mixture of the white precipitate was transferred to a Teflon flask and heated hydrothermally for 2 h at 80 °C. A white precipitate was filtered, cleaned, dried, and calcined for 2 h at 400 °C to produce ZnO rods.

2.2 Synthesized ZnO rods/ZnCo-cLDHs

ZnO/ZnCo-LDHs were synthesized using a co-precipitation method. Solution A consisted of 50 mL of $Zn(NO_3)_2$ 0.3 M and 50 mL $Co(NO_3)_2$ 0.1 M (98%; Sigma-Aldrich) in a molar ratio of Zn/Co = 3/1.[8,13] Mixture B included 1 g of ZnO dispersed evenly in a 100 mL solution of NaOH 0.5 M (96%; Xilong-China) and cetyl trimethyl ammonium bromide. Solution A was slowly added to mixture B at a steady rate of 2 mL min^{-1} and agitated using a magnetic stirrer until the reaction was complete. Throughout the process, the pH of combination B was maintained within the range of 9–10 using a 0.5 M NaOH solution. The precipitate in mixture B was stirred continuously until the pH stabilized, allowing the reaction to complete. To enhance the structure of the composite, a black precipitate was aged at 100 °C and agitated for 10 h. After filtering and rinsing the precipitate with deionized water, it was dried at 105 °C for 2 h. To prepare ZnO/ZnCo-cLDHs, ZnO/ZnCo-LDHs must be subjected to calcination at 600 °C for 4 h. Fig. S1† presents a ZnO/ZnCo-cLDHs synthesis chemical diagram.

2.3 Adsorption experiments of the prepared samples

The adsorption capability of ZnO/ZnCo-cLDHs nanocomposites was investigated using RB221. For the adsorption experiment, 0.1 g ZnO/ZnCo-cLDHs were dispersed in 100 mL RB221 80 ppm solution at pH 7.0 and shaken at 250 rpm for 100 min. At 15 min intervals, 3 mL suspensions of the samples were obtained from the reaction. After centrifugation to remove the particles, the concentration of RB221 was determined by UV-Vis absorption spectroscopy, which was calibrated using the Beer–Lambert equation at a maximum of 608 nm.

The adsorption capacity of RB221 dye (mg g^{-1}) of the nanocomposites was estimated using the following equation:[33,34]

$$q_e = \frac{C_o - C_e}{m} \times V.$$

Dye removal efficiency (H%) was calculated using the following equation:

$$H = \frac{C_o - C_e}{C_o} \times 100\%,$$

where C_o and C_e are the initial and equilibrium concentrations of RB221 (mg L^{-1}), respectively, m is the weight of the adsorbent (g), and V is the volume of the solution.

To optimize the results, the adsorption capacities of different materials, adsorbent dosage, solution pH, initial dye concentration, and contact time were examined. Additionally, a thorough investigation of the adsorption kinetics, adsorption mechanism, reusability, and desorption capacity was conducted. The concentration of RB221 was determined using a Cary 60 UV-Vis spectrophotometer (Agilent, USA).

There are many adsorption kinetic models; however, in the present study, we used first-order and intraparticle diffusion (IPD) adsorption kinetic models to study RB221 adsorption on ZnO/ZnCo-cLDHs. The first-order, second-order and IPD apparent kinetic equations were determined using the following formula:[35–37]

$$q_t = q_e(1 - e^{-k_1 t}),$$

$$q_t = \frac{k_2 q_e^2 t}{1 + k_2 q_e t},$$

$$q_t = k_{id} t^{1/2} + c,$$

where k_1 (min^{-1}) is the rate constant of the first-order apparent adsorption model and q_e and q_t (mg g^{-1}) are the adsorption capacities at equilibrium time and time t, respectively. k_2 (g mg^{-1} min^{-1}) is the rate constant of the second-order adsorption kinetic model and the apparent adsorption rate constant, k_{id} is the intraparticle diffusion constant (mg g^{-1} $min^{1/2}$), and c is the boundary layer thickness (mg g^{-1}).

2.4 Antibacterial activity

The antimicrobial activity of ZnO/ZnCo-cLDHs was further confirmed by Gram-negative bacteria (*Escherichia coli* ATCC 8739, *Pseudomonas aeruginosa* ATCC 27853, and *Salmonella typhimurium* ATCC 14028) and Gram-positive bacteria (*Staphylococcus aureus* ATCC 6538). A good diffusion method was used to assess the antibacterial capacity of ZnO/ZnCo-cLDHs.[38,39] Bacterial density was approximately 10^6–10^7 CFU mL^{-1} after activating the test bacteria with Mueller–Hinton medium for 24 h, and the bacterial density was determined *via* optical density at 660 nm wavelength. The test bacteria (100 mL) were distributed uniformly over the nutritional medium on an agar plate, followed by the utilization of a 6 mm diameter agar punch to generate wells. The wells contained 40 μL of ZnO/ZnCo-cLDHs solution with a concentration of 200–300 μg mL^{-1}. Pure water was used as the negative control, and chloramphenicol (20 μg mL^{-1}) was used as the positive control. After a 24 h incubation period at 37 °C on agar plates, the bacterial inhibition zone was determined. Diameter and image of the inhibition zone were used to record the results. The average value of three experiments was determined.

The MIC of the ZnO/ZnCo-cLDHs samples was determined using the dilution method in a 96-well microplate, and the MIC of the ZnO/ZnCo-cLDHs samples was examined.[38] Each well contained 100 μL of bacterial medium and 100 μL of ZnO/ZnCo-cLDHs samples dispersed in water at concentrations from 50 to −1000 μg mL^{-1}. After 24 h of incubation at 37 °C, 20 μL 0.01% resazurin reagent was added to each well. The color shift and MIC value were noted. The outcomes were observed and it was found that the resazurin indicator was blue in the solution. Bacterial growth was observed in wells where the resazurin solution turned pink instead of blue. The lowest concentration of ZnO/ZnCo-cLDHs samples in the investigated concentration range that can stop bacterial growth (without discoloring resazurin) is known as the MIC.

3. Results and discussion

3.1 Characterization

Fig. 1A and B display the X-ray diffraction (XRD; Bruker Germany) data of three samples: ZnO, ZnCo-cLDHs, and ZnO/ZnCo-cLDHs.

Peaks in the ZnCo-cLDHs correspond to the hexagonal ZnO phase at 31.86°; 34.44°; 36.66°; 47.9°; 56.87°; 63.2°; 68.12°; and 69.11° (JCPDS no. 36-1451)[40,41] and the spinel $ZnCo_2O_4$ phase at 31.44°; 36.82°; 38.26°; 44.71°; 55.52°; 59.11°; and 65.67° (JCPDS no. 23-1390)[42,43] (Fig. 1A). Moreover, the ZnCo-cLDHs sample peak at 31.79° includes two peaks at 31.86° and 36.44° for the ZnO and $ZnCo_2O_4$ phases, respectively, while the peak at 36.76° includes two peaks at 36.66° and 36.82° for the ZnO and $ZnCo_2O_4$ phases, respectively. This finding aligns with the thermal degradation of LDHs to produce MMO.[24,44,45] For instance, Bayu Wiyantoko heated MgAl-LDHs at 400 °C to produce a mixture of MgO and $MgAl_2O_4$.[46] The peaks of the ZnO/ZnCo-cLDHs and ZnCo-cLDHs samples were comparable. There was a minor shift in the peaks at 31.79°, 34.45°, and 36.76° for ZnCo-cLDHs because of the higher amount of ZnO in the ZnO/ZnCo-cLDHs samples, indicating an interaction between ZnO and ZnCo-cLDHs (Fig. 1B).

The peaks at 3446 and 1625 cm^{-1} are indicative of the vibration of the OH^- group in water,[47] whereas the peak at 1330 cm^{-1} corresponds to the vibration of the NO_3^- group in the interlayer, as shown in the FT-IR (Bruker Tensor 27) spectra of the samples (Fig. 1C). This result indicates that ZnCo-cLDHs and ZnO/ZnCo-cLDHs did not completely decompose into mixed oxides. The stretching vibrations of the Zn–O and Co–O bonds are represented by the peaks that appear at 663 cm^{-1} and 500 cm^{-1} in the oxide mixture, respectively.[48,49]

Scanning electron microscopy (SEM; S-4800 device HITACHI) images (Fig. 2A–C) were used to analyze the morphologies of ZnO, ZnCo-cLDHs, and ZnO/ZnCo-cLDHs. The SEM image of pure ZnO shows rods-like morphology with an average diameter of approximately 140 nm and length of 0.5–1 μm (Fig. 2A). The ZnCo-cLDHs were composed of thin, multilayered nanoparticles with diameters ranging from approximately 70 to 100 nm (Fig. 2B). The precipitation of ZnCo-cLDHs onto the ZnO surface yielded SEM images that unequivocally illustrated the dispersion of ZnCo-cLDHs nanolayers across the rod-shaped ZnO surface (Fig. 2C). At this juncture, ZnO rods can function as stationary columns to separate ZnCo-cLDHs nanolayers, thereby augmenting the contact area and porous structure of ZnO/ZnCo-cLDHs.

High-resolution transmission electron microscopy (HRTEM; JEOL JEM 2100) images (Fig. 2D) revealed that the ZnCo-cLDHs layered nanosheet uniformly covered the ZnO rods, causing their formerly smooth surfaces to become rough. In addition to depicting the heterojunction interface between the ZnO rods and ZnCo-cLDHs, the HRTEM images of ZnO/ZnCo-cLDHs reveal the lattice edge spacing (0.245 nm), which corresponds to the (311) planes of $ZnCo_2O_4$.[50,51]

The elemental distributions of Co, O, and Zn in ZnCo-cLDHs and ZnO/ZnCo-cLDHs were observed by energy-dispersive X-ray spectroscopy (EDX; S-4800 Hitachi). Elemental O (24.18 wt%), Co (17.44 wt%), and Zn (58.38 wt%) were present in ZnCo-cLDHs samples (Fig. 3A), while O (23.83 wt%), Co (8.78 wt%), and Zn (67.39 wt%) were found in ZnO/ZnCo-cLDHs samples (Fig. 3B). Compared to that in ZnCo-cLDHs, the Zn signal in the ZnO/ZnCo-cLDHs samples was noticeably stronger (Fig. 3C and D).

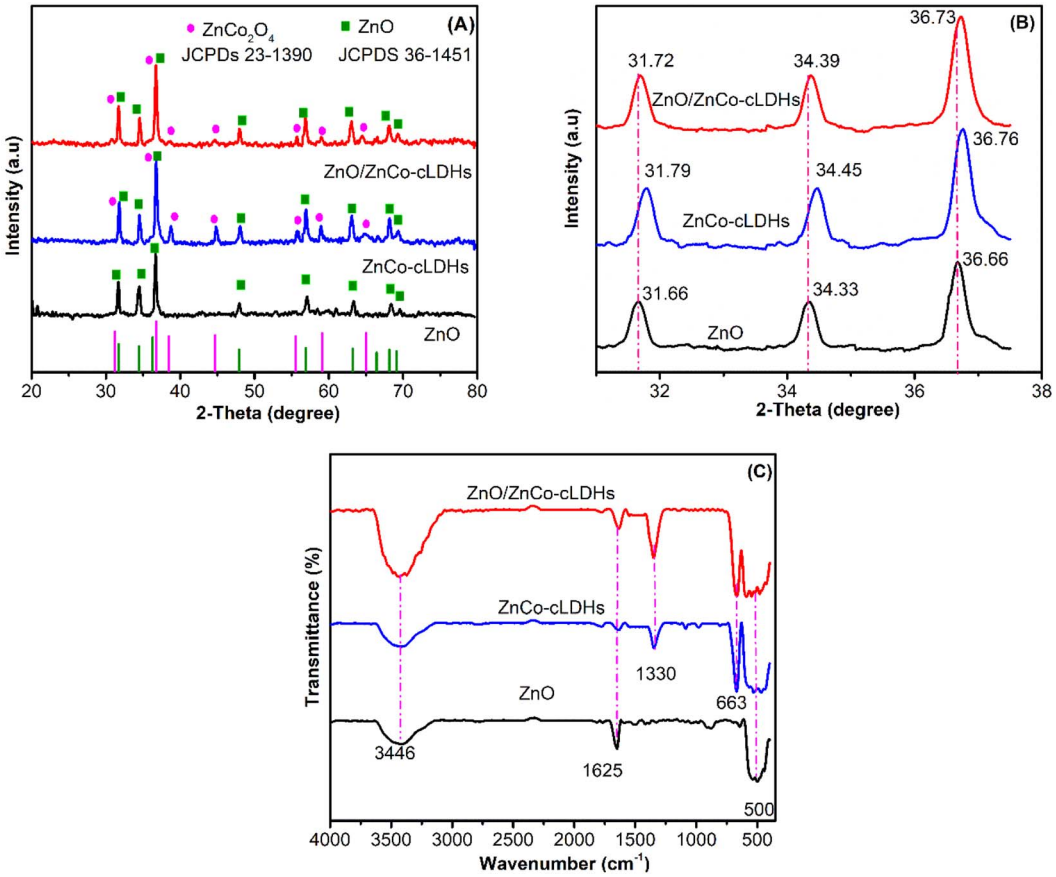

Fig. 1 XRD patterns (A and B) and FTIR spectra (C) of ZnO, ZnCo-cLDHs, and ZnO/ZnCo-cLDHs.

A comprehensive analysis of the chemical states of the as-prepared ZnO/ZnCo-cLDHs was conducted using XPS (ULVAC-PHI). The full XPS spectrum of the ZnO/ZnCo-cLDHs sample comprises zinc (Zn), oxygen (O), and cobalt (Co), with no other elements present, allowing for the precise determination of its composition based on the precursor (Fig. 4A). Two energy levels, 1021.28 and 1044.54 eV, which correspond to $2p_{1/2}$ and $2p_{3/2}$ of Zn 2p, are shown in high-resolution in Fig. 4B.[31,50] Two peaks at 855.4 and 873.3 eV in the Co 2p spectrum (Fig. 4C) corresponded to Co $2p_{1/2}$ and Co $2p_{3/2}$, respectively. Deconvolution of the two peaks Co $2p_{1/2}$ and Co $2p_{3/2}$ yielded four peaks at 780.75; 795.54 and 779.37; 794.36 eV, all of which correspond to Co^{2+} and Co^{3+}, respectively.[31,52] Additional satellite peaks suggest that Co exists in a multivalent state. Three peaks at 529.4, 530.4, and 531.6 eV, which correspond to oxygen vacancies, metal–oxygen bonds, and chemisorbed oxygen species[53] on the surface of ZnO/ZnCo-cLDHs, respectively, were revealed by deconvolution of the O 1s peak (Fig. 4D).

The Brunauer–Emmett–Teller (BET) and BJH methods calculated the specific surface areas and the mesoporous distributions. Particle size, pore volume, and specific surface area are factors that affect adsorption capacity.[54] Fig. 5A illustrates the nitrogen adsorption–desorption isotherms of the ZnO, ZnCo-cLDHs, and ZnO/ZnCo-cLDHs samples. Analytical results indicate that the adsorption and desorption curves correspond to type IV isotherms, which suggests that porous materials predominate the adsorption process. Furthermore, the adsorption branches of the isotherms were located beneath the desorption branches. The distinct presence of a hysteresis loop in each isotherm indicates that the narrowing of pores hinders the release of nitrogen during desorption.[55] The ZnCo-cLDHs samples have the following values: BET 18.584 ($m^2\ g^{-1}$), pore volume 0.148 ($cm^3\ g^{-1}$), and average pore size of 22.33 nm (Fig. 5B and Table 1).

The ZnO/ZnCo-cLDHs samples showed an increase in BET (from 18.584 to 20.678 $cm^2\ g^{-1}$) and pore volume (from 0.148 to 0.195 $cm^3\ g^{-1}$). The pore sizes of ZnCo-cLDHs and ZnO/ZnCo-cLDHs were distributed mostly between 20 and 30 nm (Table 1). Thus, the combination of ZnO and ZnCo-cLDHs enhanced the porosity and surface area of ZnO/ZnCo-cLDHs.

3.2 Batch adsorption behavior

3.2.1 Adsorption capacities of different materials and contact times. Fig. 6A illustrates the adsorption capability of RB221 onto ZnO, ZnCo-cLDHs, and ZnO/ZnCo-cLDHs as a function of contact times. According to the findings, the RB221 adsorption capability of the ZnO, ZnCo-cLDHs, and ZnO/ZnCo-cLDHs samples were 53.2, 63.02, and 75.74 mg g^{-1} at 100 minutes, respectively. After 25 min, the adsorption of RB221 on the ZnO/ZnCo-cLDHs samples increased significantly,

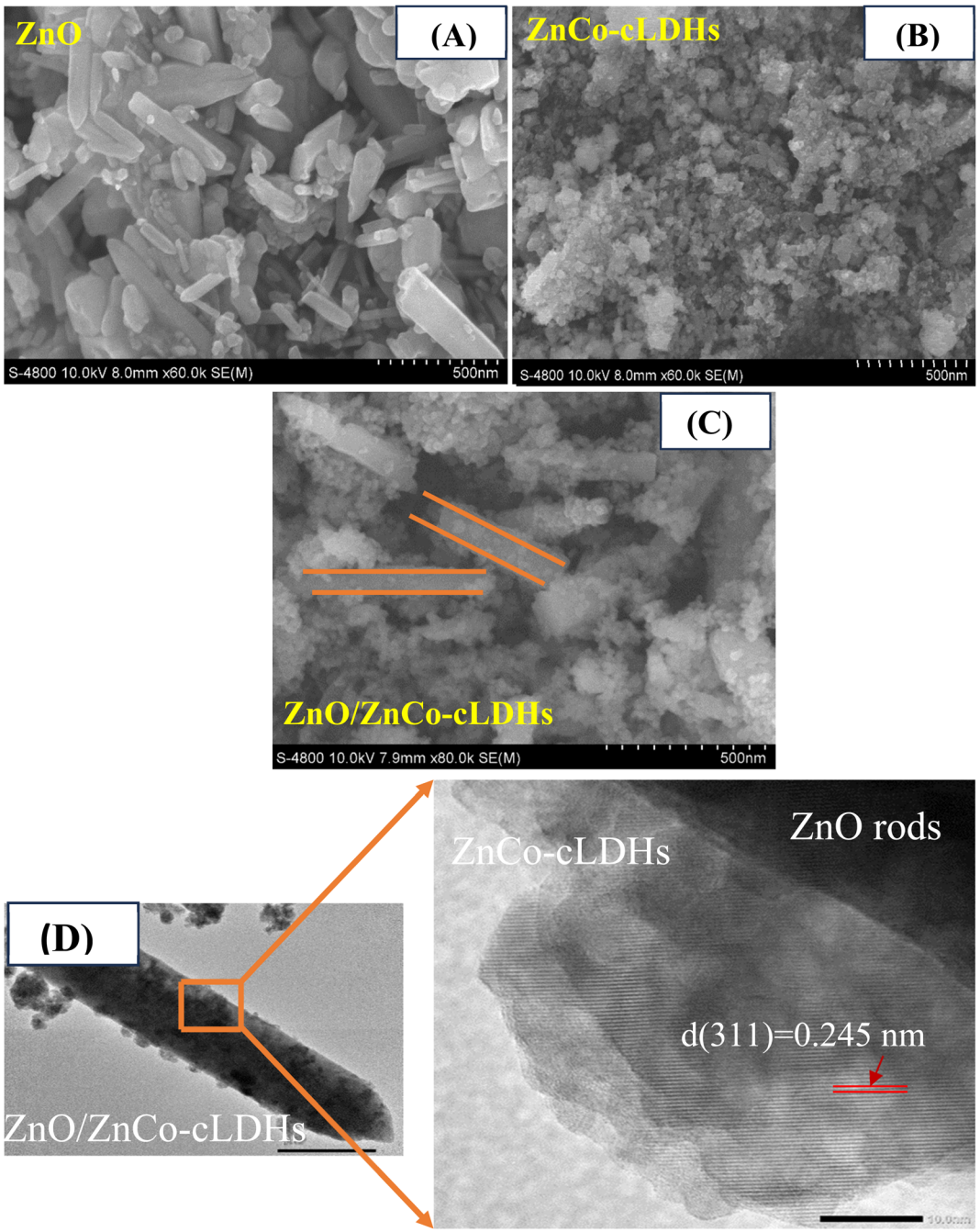

Fig. 2 SEM images of (A) ZnO, (B) ZnCo-cLDH, and (C) ZnO/ZnCo-cLDH samples. TEM and HRTEM images of (D) ZnO/ZnCo-cLDHs.

approaching an adsorption capacity of 72.23 mg g^{-1}. This is because early in the process, cLDHs composed of MMO (ZnO and $ZnCo_2O_4$) are exposed to external anions, which can introduce guest anions and rebuild the structure of their layers.[13,56] The ZnO/ZnCo-cLDHs can remove the RB221 solution through two distinct mechanisms: adsorption and reconstruction of calcined precursor intercalation.[8,57,58] The XRD results show that the ZnCo-cLDHs are ZnO and $ZnCo_2O_4$. The MMO produced during the calcination of LDHs possess a unique property: the capacity to reconstruct the LDHs structure with anions in aqueous solution *via* the "memory effect" mechanism.[13,18] As RB221 is an anionic dye, the ZnCo-cLDHs rebuild the ZnCo-LDHs layer structure by incorporating the targeted RB221 anions into the interlayers when present in water. Furthermore, the RB221 anion could interact electrostatically with the positively charged MMO adsorption sites.[13,59] The SEM and BET results of the ZnO/ZnCo-cLDHs showed that the ZnO rods could spread the ZnCo-cLDHs nanolayers, thereby expanding the contact area of the ZnO/ZnCo-cLDHs and enhancing the adsorption ability of the composites. A selection of recent studies on composites from cLDHs for pollution treatment is shown in Table 2.

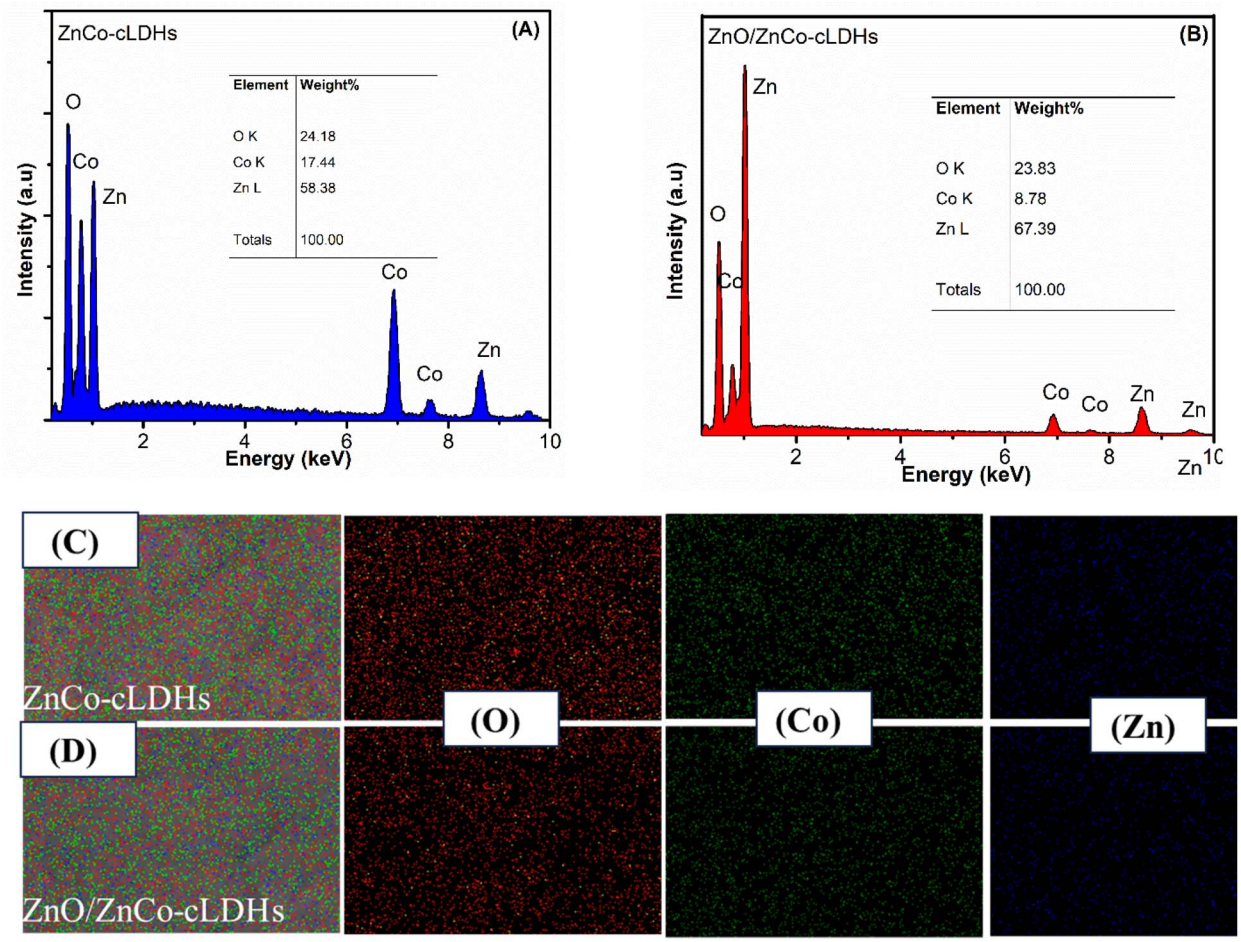

Fig. 3 EDX spectra (A and B) and EDX mapping (C and D) of ZnCo-cLDHs and ZnO/ZnCo-cLDHs.

After 100 min, the highest adsorption capacity of RB221 onto ZnO/ZnCo-cLDHs was 75.74 mg g^{-1}, indicating that the adsorption process was not significantly variable. The ZnO/ZnCo-cLDHs were almost at adsorption/desorption equilibrium at this stage. Consequently, the number of active sites on the adsorbent was reduced, leading to a negligible increase in the adsorption capacity.

3.2.2 Influence of the initial concentration. The effect of initial dye concentration on the adsorption capacity of the ZnO/ZnCo-cLDHs is shown in Fig. 6B. The adsorption capacity increased from 39 to 76.33 mg g^{-1} when the RB221 concentration was increased from 40 to 90 ppm. The adsorption capacity was also affected by the initial adsorbate concentration. Adsorption reaches equilibrium quickly when the initial concentration is low, whereas it takes longer to reach equilibrium when the initial concentration is high.[44,62] As the initial concentration increased, the capacity of the adsorbent also increased, which enhanced mass transfer and diffusion from the solution to the adsorbent's free surface.[5,10]

3.2.3 Effect of adsorbent dosage. The dosage of the ZnO/ZnCo-cLDHs adsorbent was studied by changing it from 0.5 to 1.75 g L^{-1} for treating RB221 dye while keeping the other parameters as follows: $C_o = 80$ mg L^{-1}, pH = 7, and contact time = 100 min. As the ZnO/ZnCo-cLDHs dose was increased from 0.5 to 1.75 g L^{-1}, as shown in Fig. 6C, the RB221 removal efficiency rose but RB221 adsorption capacity was reduced. For example, the adsorption capacity increased to 88.08 mg g^{-1} at a ZnO/ZnCo-cLDHs dose of 0.5 g L^{-1}; however, the adsorption efficiency was only 55.4%. At a dosage of 1.75 g L^{-1}, the adsorption capacity decreased to 44.74 mg g^{-1}; however, the adsorption efficiency reached 97.7%. The decrease in the adsorption capacity with increasing ZnO/ZnCo-cLDHs dose is attributed to the likelihood of collisions and aggregation among solid particles, resulting in a reduction in the effective surface area per unit weight (g) of the adsorbent.[63,64] Based on removal efficiency and adsorption capacity, a dosage of 1.0 g L^{-1} was considered optimal for subsequent trials.

3.2.4 Effect of initial pH. Using various pH values between 5 and 9, effects of the solution pH on the adsorption capacity of ZnO/ZnCo-cLDHs were investigated (Fig. 6D); when the pH of the solution was increased from 5 to 7, the adsorption capacity of ZnO/ZnCo-cLDHs increased significantly; however, it decreased from 8 to 9. The highest adsorption capacity was achieved at pH 7 (75.74 mg g^{-1}). The ZnO/ZnCo-cLDHs surface displayed a positive charge when the pH of the dye solution ranged from 5 to 7, which was below the point of zero charge

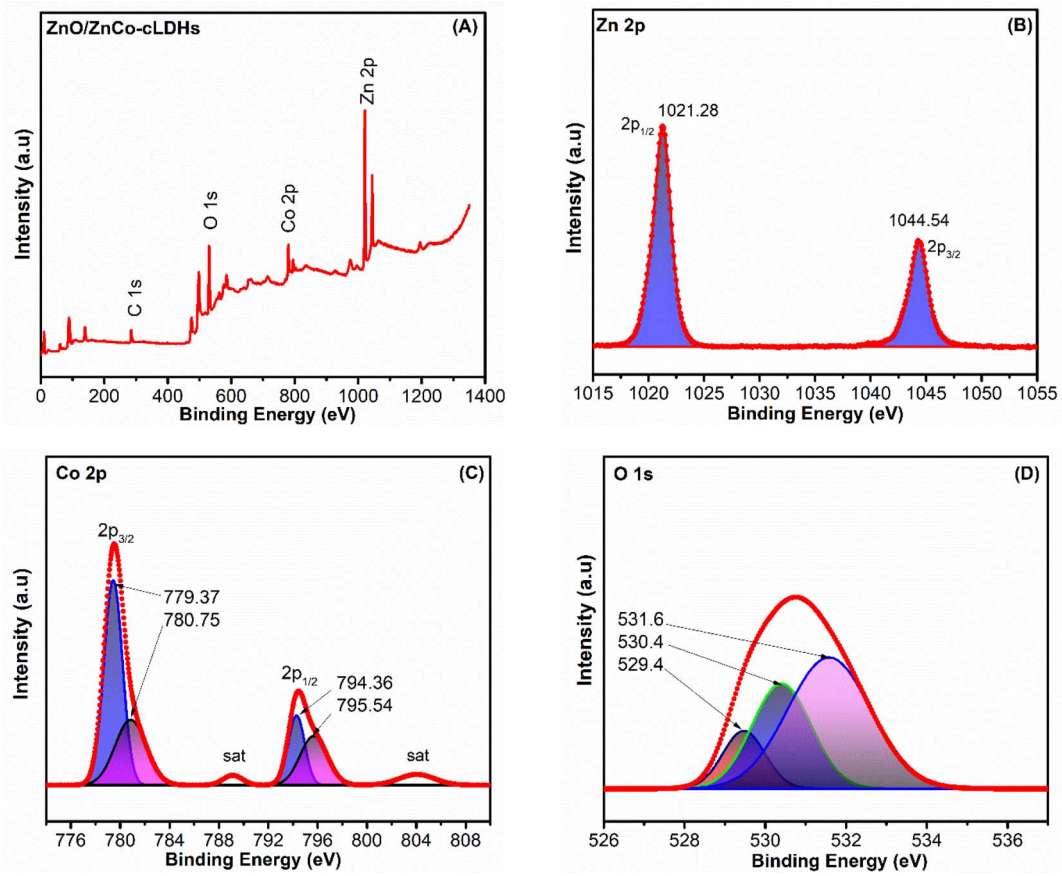

Fig. 4 Full XPS spectrum (A) of ZnO/ZnCo-cLDH composites. High-resolution XPS spectrum of (B) Zn 2p, (C) Co 2p, and (D) O 1s spectra of ZnO/ZnCo-cLDH composites.

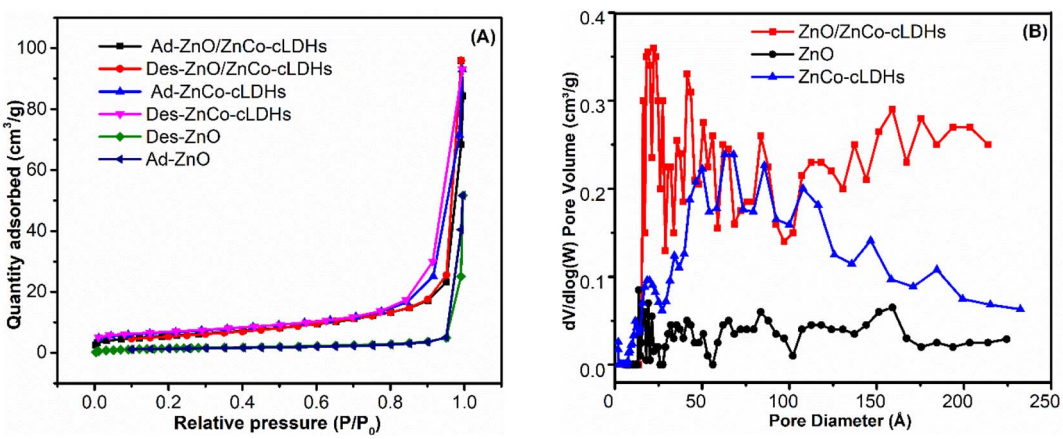

Fig. 5 (A) Nitrogen adsorption–desorption isotherms of ZnO, ZnCo-cLDH and ZnO/ZnCo-cLDH samples. (B) Average pore diameter, pore volume, and pore diameter distribution of ZnO, ZnCo-cLDH and ZnO/ZnCo-cLDH samples.

(pH_{zpc}).[64,65] The pH_{pzc} of ZnO/ZnCo-cLDHs was found to be 7.7. Furthermore, RB221 is classified as an anionic dye, resulting in attractive interactions between ZnO/ZnCo-cLDHs and the RB221 anion. Consequently, this interaction leads to an increase in the adsorption capacity of ZnO/ZnCo-cLDHs. At a pH of 8–9, above the pH_{zpc}, the surface of ZnO/ZnCo-cLDHs acquires a negative charge;[44,65] as a result, there is an electrostatic attraction between ZnO/ZnCo-cLDHs and the anion RB221, leading to a decrease in the adsorption capacity of ZnO/ZnCo-cLDHs.

3.2.5 Recyclability performance. Adsorbent selectivity and stability are primarily determined by their efficiency and

Table 1 Specific surface area, pore volume, and average pore size of ZnO, ZnCo-cLDHs, and ZnO/ZnCo-cLDHs

Samples	S_{BET} ($m^2\ g^{-1}$)	Pore volume ($cm^3\ g^{-1}$)	Average pore size (nm)
ZnO	5.1893	0.062	24.94
ZnCo-cLDHs	18.584	0.1480	30.59
ZnO/ZnCo-cLDHs	20.678	0.195	22.33

reusability across several adsorption cycles.[8,18] The ZnO/ZnCo-cLDHs samples were subjected to dye adsorption under the best conditions that could be explored, including an RB221 concentration of 80 ppm, adsorption time of 100 minutes, loading amount of 1 g L^{-1}, and pH 7. The ZnO/ZnCo-cLDHs that were adsorbed were subjected to drying and desorption using a desorption solution consisting of NaOH and ethanol in a 1 : 1 ratio, with a volume of 20 mL for 60 min. Following desorption, ZnO/ZnCo-cLDHs were rinsed with distilled water, dried at 100 °C, and subsequently reused for RB221 adsorption under the aforementioned conditions. The adsorption capability of RB221 onto ZnO/ZnCo-cLDHs decreases progressively with each reuse, with success rates of 75.74; 71.64; 67.15, and 61.89 mg g^{-1} after four reuses, respectively.

3.2.6 Application of kinetic models to the adsorption data. Pseudo-first-order, pseudo-second-order and IPD models were used to simulate the adsorption experimental data to determine the adsorption kinetics of RB221 on ZnO/ZnCo-cLDHs.

Fig. 7 and Table 3 display the kinetic parameters of RB221 adsorption on ZnO/ZnCo-cLDHs, including the correlation coefficients R, q_e, rate constant (k), and k_{id}. According to these findings, the lines linked to the pseudo-first-order model for RB221 did not match the adsorption kinetics data as well as the straight lines fitted by the pseudo-second-order model (Fig. 7A and B). The pseudo-second-order kinetic model of RB221 for ZnO/ZnCo-cLDHs demonstrated a correlation coefficient of $R^2 = 0.99599$. Additionally, the $q_e = 79.05$ mg g^{-1} value obtained from this model closely matched the experimental value ($q_{e,exp} = 75.74$ mg g^{-1}), indicating a good agreement.[3]

The linear fitting of the IPD model in Fig. 7C indicates that the line does not meet the origin, implying that intraparticle diffusion is not the only rate-controlling step.[36,37] The adsorption of RB221 dye onto ZnO/ZnCo-cLDHs involves many phases,

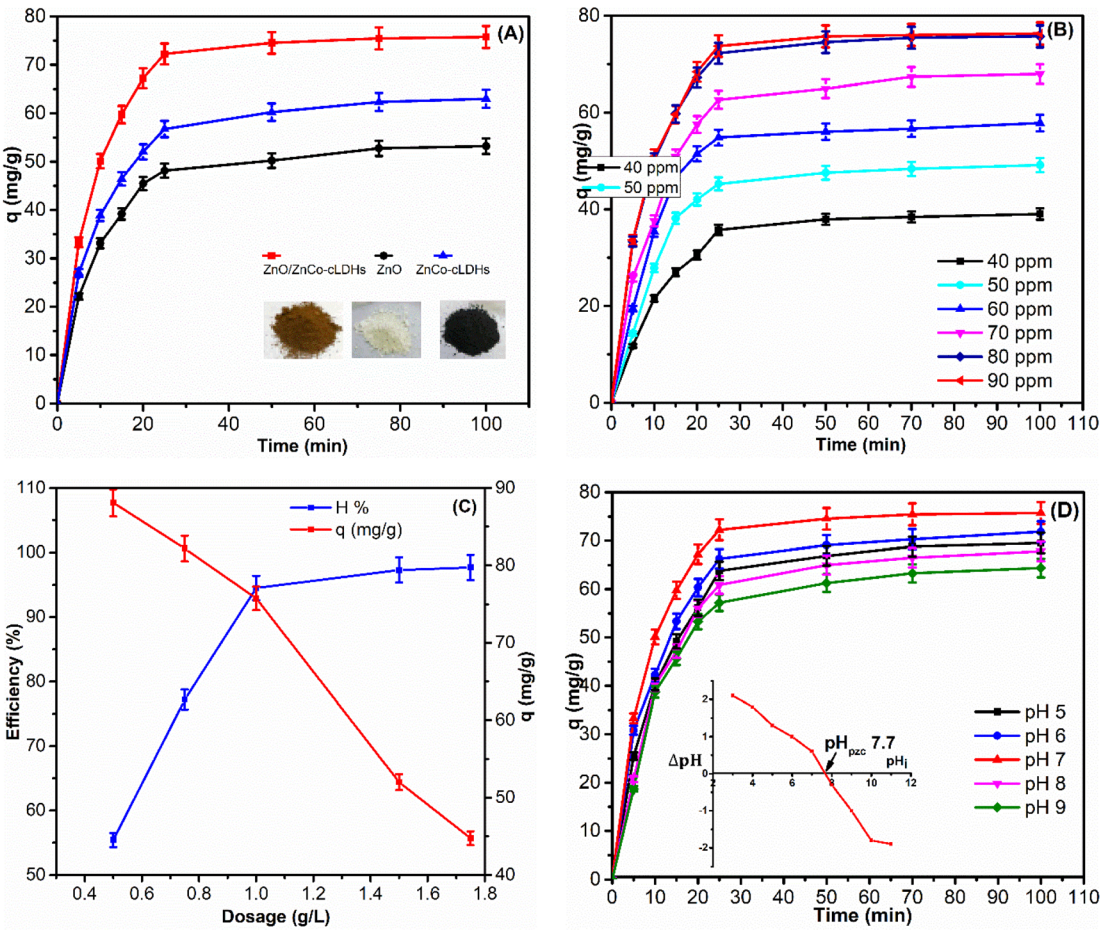

Fig. 6 (A) Adsorption capacities of different materials and contact time (RB221 initial concentration of 80 ppm, adsorbent dosage of 1.0 g L^{-1}, and pH 7). (B) Influence of initial concentration (C_o = 40–90 ppm, dosage of ZnO/ZnCo-cLDHs of 1.0 g L^{-1}, and pH 7). (C) Effect of adsorbent dosage (C_o = 80 ppm, dosage of ZnO/ZnCo-cLDHs from 0.5–1.75 g L^{-1}, and pH 7). (D) Effect of initial pH (C_o = 80 ppm, dosage of ZnO/ZnCo-cLDHs of 1.0 g L^{-1}, and pH 5–9).

Table 2 Comparison of the pollutant treatment ability of ZnO/ZnCo-cLDHs with composites from cLDHs

Composites	Pollutants	Adsorption capacities (mg g^{-1})	Reference
ZnO/MgAl-cLDHs	Acid red G	91.1	17
CuAl-cLDH/CNT/PVDF	Carminic acid	33.44	59
MnO_2/MgFe-cLDHs	As(III)	51.03	60
GCN/CaAl-cLDHs	U(VI)	196.69	21
SWCNT/MgAl-cLDHs	Phenol	219.0	61
SWCNT/MgAl-cLDHs	4-Chlorophenol	255.6	61
ZnO/ZnCo-cLDHs	Reactive Blue 221	This work	

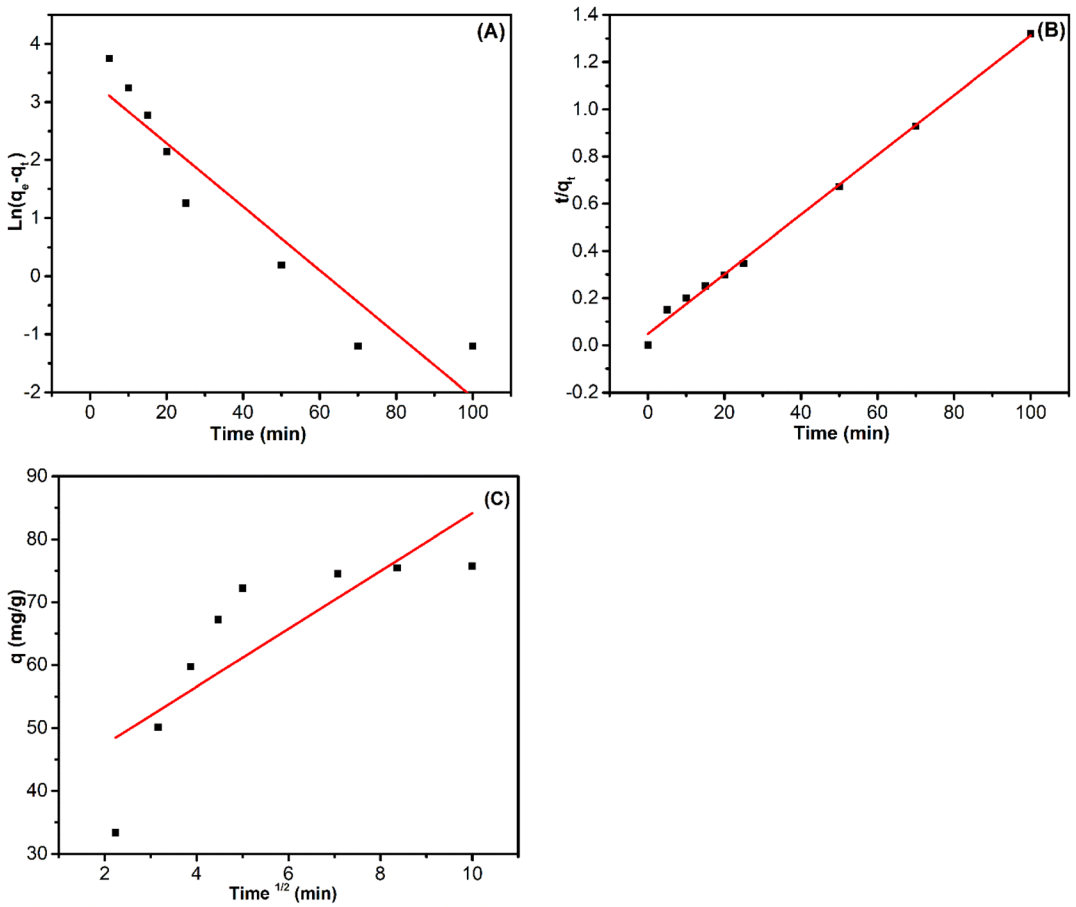

Fig. 7 Experimental data obtained from the linear fitting (A) the pseudo-first-order kinetic, (B) pseudo-second-order kinetic and (C) IPD models for RB221 adsorption on ZnO/ZnCo-cLDHs.

including the diffusion adsorption stage, intra-particle diffusion stage, and equilibrium adsorption stage.[3,34,66]

3.2.7 Equilibrium isotherms. An isotherm curve illustrates the dynamic equilibrium relationship between adsorbate concentration and adsorption capacity at a specific temperature.[21,44] Freundlich and Langmuir equations were applied to determine the dynamic equilibrium relationship between RB221 concentration and ZnO/ZnCo-cLDHs adsorption capacity. The non-linear form of the Langmuir adsorption isotherm model can be expressed as[16]

$$\frac{C_e}{q_e} = \frac{C_e}{q_m} + \frac{1}{q_m K_L},$$

where C_e is the RR221 equilibrium concentration in the solution (mg L^{-1}), q_m is the maximum adsorption capacity for solute uptake (mg g^{-1}), and K_L is the equilibrium Langmuir constant.

The Freundlich isotherm model is represented by the equation below:[16,67]

$$\ln q_e = \frac{1}{n}\ln C_e + \ln K_F.$$

Table 3 Kinetic parameters for adsorption of RB221 on ZnO/ZnCo-cLDHs

	Pseudo-first order			Pseudo-second order		
$q_{e(exp)}$	q_e (mg g^{-1})	k_1	R^2	q_e (mg g^{-1})	k_2	R^2
75.74	29.41	0.000547	0.877090	79.5	0.01265	0.99599

Intra-particle diffusion		
k_{id} (mg g^{-1} min$^{1/2}$)	C (mg g^{-1})	R^2
4.594	38.176	0.615

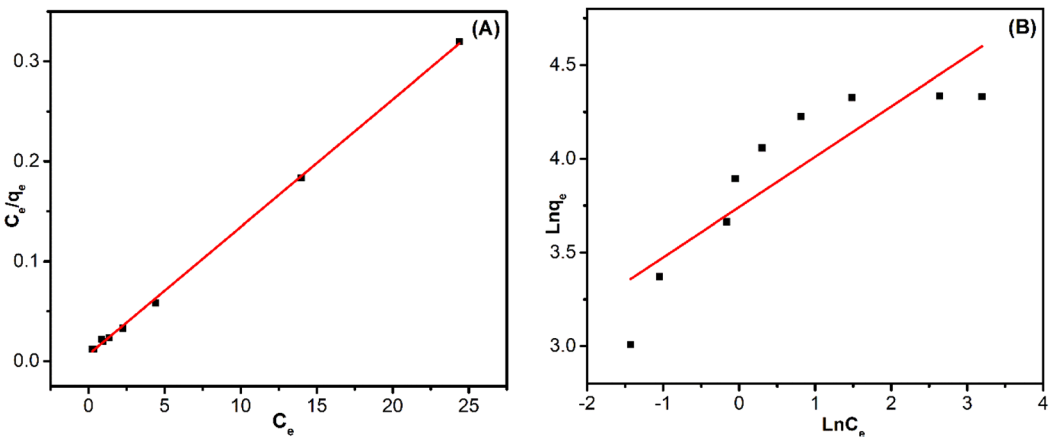

Fig. 8 Experimental data obtained from the linear fitting of (A) Langmuir and (B) Freundlich isotherms for RB221 adsorption on ZnO/ZnCo-cLDHs.

Table 4 Isotherm model constants and correlation coefficients for RB221 adsorption

	Langmuir			Freundlich		
q_m (mg g^{-1})	K_L (L mg^{-1})	R_L	R^2	K_F (mg g^{-1}) (L mg^{-1})$^{1/n}$	n	R^2
78.3699	1.90732	0.007366	0.99852	42.27198	3.72287	0.74604

Here, K_F and $1/n$ are the Freundlich constant and adsorption intensities, respectively.

The parameters obtained from these isotherms are listed in Fig. 8A, B and Table 4. Based on the determined parameters, it is clear that the Langmuir model is a better fit for the experimental data in the adsorption process of RB221 onto ZnO/ZnCo-cLDHs. This is supported by the higher correlation coefficient (R^2 = 0.99852) of the Langmuir model than that of the Freundlich isotherm (R^2 = 0.74604). According to Langmuir isotherms, the monolayer adsorption capacity (q_L) of RB221 onto ZnO/ZnCo-cLDHs was estimated to be 78.3699 mg g^{-1}; this value was found to be compatible with the experimental values ($q_{e(exp)}$ = 75.74 mg g^{-1}). The same results were verified by other authors when they examined dye adsorption isotherms in calcined LDHs materials, which are the adsorption mechanisms of monolayer absorption and chemisorption processes.[12,22,68,69]

3.3 Results of the antibacterial assay

The data shown in Fig. 9 and Table 5 indicate that ZnO/ZnCo-cLDHs at doses of 200–300 μg mL^{-1} can eradicate bacteria. ZnO/ZnCo-cLDHs have a moderate level of antibacterial activity, as evidenced by inhibition zones measuring 8–9 mm, and a weaker inhibition zone of less than 8 mm at doses of 200–300 μg mL^{-1}. Smaller and more surface area nanoparticles are more likely to stick to the bacterial cell wall, which releases a variety of reactive oxygen species (ROS) and eventually destroys bacterial cells.[23,70,71] The antibacterial efficacy of nanomaterials is intricately linked to their size, existence of charged moieties, presence of sharp boundaries, and occurrence of the orthorhombic phase.[70–72]

The ZnO/ZnCo-cLDHs samples were diluted to different concentrations, ranging from 50 to 1000 μg mL^{-1} (Table 6). The minimum inhibitory concentration (MIC) values for the ZnO/ZnCo-cLDHs samples against *E. coli*, *S. aureus*, *P. aeruginosa*,

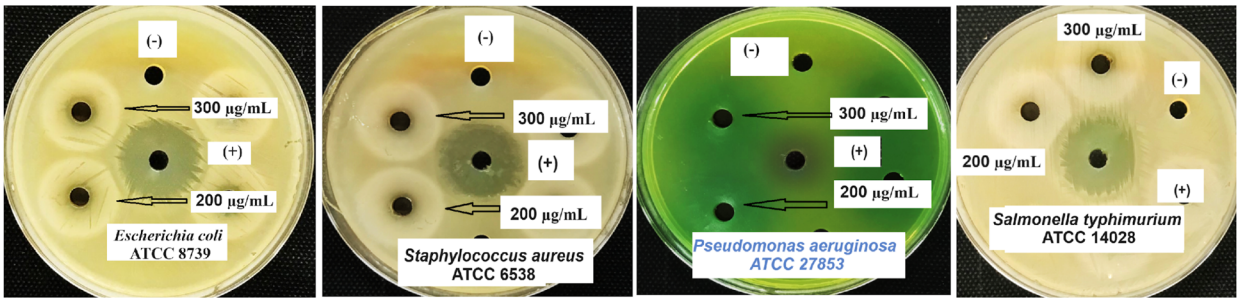

Fig. 9 Zone of inhibition produced of ZnO/ZnCo-cLDHs against *E. Coli*, *S. aureus*, *P. aeruginosa*, and *S. typhimurium*.

Table 5 Antibacterial activity of ZnO/ZnCo-cLDHs against some bacteria

	Zone (mm)			
Samples	*E. coli*	*S. aureus*	*P. aeruginosa*	*S. typhimurium*
ZnO/ZnCo-cLDHs 200 (μg mL^{-1})	8.0 ± 0.2	8.0 ± 0.1	6.0 ± 0.0	6.0 ± 0.0
ZnO/ZnCo-cLDHs 300 (μg mL^{-1})	9.0 ± 0.1	8.6 ± 0.1	6.0 ± 0.0	8.0 ± 0.0
Chloramphenicol (20 μg)	**24.0 ± 0.2**	**24.0 ± 0.1**	**15.0 ± 0.1**	**21.0 ± 0.2**

Table 6 MIC values of ZnO/ZnCo-cLDHs samples against bacteria

	MIC (μg mL^{-1})			
Samples	*E. coli*	*S. aureus*	*P. aeruginosa*	*S. typhimurium*
ZnO/ZnCo-cLDHs	175	175	450	275
Chloramphenicol (ppm)	**0.2**	**0.2**	**0.2**	**0.2**

and *S. typhimurium* were 175, 175, 450, and 275 μg mL^{-1}, respectively. When compared to the positive control, chloramphenicol at a concentration of 0.2 ppm, the sample's MIC findings were substantially lower.

4. Conclusions

ZnO rods, ZnCo-cLDHs, and ZnO/ZnCo-cLDHs were successfully synthesized. A mixture of ZnO and $ZnCo_2O_4$ oxides, following the calcination of ZnCo-LDHs, exhibits excellent dispersion on the surface of ZnO rods. Under ideal conditions, an adsorption duration of 100 min, adsorbent loading of 1.0 g L^{-1}, initial RB221 concentration of 80 ppm, and pH of 7 allowed ZnO/ZnCo-cLDHs to reach an adsorption capacity of 75.74 mg g^{-1} for the RB221 dye. The adsorption capacity for RB221 adsorption onto ZnO/ZnCo-cLDHs declined to 61.89 mg g^{-1} after four reuse cycles. Experimental results of tissue determination yielded first-order and second-order kinetic equations. RB221 adsorption on the ZnO/ZnCo-cLDHs was in good agreement with the Langmuir isotherm model. The ZnO/ZnCo-cLDHs composite exhibited a larger zone of inhibition against Gram-positive *S. aureus* bacteria than against Gram-negative *E. coli* when assessed using a standard inhibitory microbiology test with a diameter of 6 mm.

Data availability

Data, including origin files, for the article titled "Synthesis of calcined LDHs materials decorated on ZnO nanorods: enhancing adsorption capacity and antibacterial activity" are available at **https://doi.org/10.6084/m9.figshare.28080734**.

Conflicts of interest

There are no conflicts to declare.

References

1 T. H. A. Nguyen, D. T. Quang, L. Van Tan and T. K. Vo, *RSC Adv.*, 2023, **13**, 5859–5868.
2 C. W. Chiu, M. T. Wu, C. L. Lin, J. W. Li, C. Y. Huang, Y. C. Soong, J. C. M. Lee, W. A. L. Sanchez and H. Y. Lin, *Nanomaterials*, 2020, **10**, 748, DOI: **10.3390/nano10040748**.
3 B. Saha, G. Shil, A. Debnath and B. Saha, *J. Indian Chem. Soc.*, 2024, **101**, 101407, DOI: **10.1016/j.jics.2024.101407**.
4 R. Pandimurugan and S. Thambidurai, *J. Environ. Chem. Eng.*, 2016, **4**, 1332–1347.

5 A. L. Johnston, E. Lester, O. Williams and R. L. Gomes, *J. Environ. Chem. Eng.*, 2021, **9**, 105197, DOI: **10.1016/j.jece.2021.105197**.
6 G. Yuvaraja, C. Prasad, Y. Vijaya and M. V. Subbaiah, *Int. J. Ind. Chem.*, 2018, **9**, 17–25.
7 M. Cheng, G. Zeng, D. Huang, C. Lai, P. Xu, C. Zhang and Y. Liu, *Chem. Eng. J.*, 2016, **284**, 582–598.
8 B. Wiyantoko, P. Kurniawati, T. E. Purbaningtias, M. H. Jauhari, A. Yahya, M. Tamyiz, I. Fatimah and R. A. Doong, *Mater. Res. Express*, 2022, **9**, 035505, DOI: **10.1088/2053-1591/ac5ef7**.
9 Y. Shi, X. Wang, C. Feng, W. Chen and S. Yang, *ACS Omega*, 2024, **9**, 573–584.
10 E. E. Abdel-Hady, H. F. M. Mohamed, S. H. M. Hafez, A. M. M. Fahmy, A. Magdy, A. S. Mohamed, E. O. Ali, H. R. Abdelhamed and O. M. Mahmoud, *Sci. Rep.*, 2023, **13**, 6435, DOI: **10.1038/s41598-023-33142-x**.
11 C. Wang, Z. Wang, J. Xu and Y. Nie, *ACS Omega*, 2021, **6**, 22126–22136.
12 S. Li, Y. Yang, S. Huang, Z. He, C. Li, D. Li, B. Ke, C. Lai and Q. Peng, *Appl. Clay Sci.*, 2020, **188**, 105414, DOI: **10.1016/j.clay.2019.105414**.
13 B. A. Jiménez-López, R. Leyva-Ramos, J. J. Salazar-Rábago, A. Jacobo-Azuara and A. Aragón-Piña, *Environ. Nanotechnol., Monit. Manage.*, 2021, 100580.
14 C. Jiehu, W. Chunlei, Z. Ming, Z. Jie, F. Li, D. Xiuhong, C. Leiming and L. Chunguang, *Appl. Surf. Sci.*, 2020, **534**, 147564, DOI: **10.1016/j.apsusc.2020.147564**.
15 L. Guo, Y. Wu, P. Duan and Z. Zhang, *Constr. Build. Mater.*, 2020, **232**, 117256, DOI: **10.1016/j.conbuildmat.2019.117256**.
16 T. Zhang, Y. Zhou, M. He, Y. Zhu, X. Bu and Y. Wang, *Chem. Eng. J.*, 2013, **219**, 278–285.
17 S. Yuan, Y. Li, Q. Zhang and H. Wang, *Colloids Surf., A*, 2009, **348**, 76–81.
18 M. Daud, A. Hai, F. Banat, M. B. Wazir, M. Habib, G. Bharath and M. A. Al-Harthi, *J. Mol. Liq.*, 2019, **288**, 110989.
19 Y. Huang, C. Liu, S. Rad, H. He and L. Qin, *Processes*, 2022, **10**(4), 617.
20 A. M. Cardinale, C. Carbone, S. Molinari, G. Salviulo and F. Ardini, *Chemistry*, 2023, **5**, 633–645.
21 Z. H. Momin, L. P. Lingamdinne, R. Kulkarni, C. A. K. Pal, Y. L. Choi, J. R. Koduru and Y. Y. Chang, *Chemosphere*, 2024, **346**, 140551, DOI: **10.1016/j.chemosphere.2023.140551**.
22 P. Yarahmadi, M. Movahedi and H. Salavati, *Phys. Chem. Res.*, 2021, **9**, 311–325.
23 J. Miao, X. Zhao, Y. X. Zhang and Z. H. Liu, *J. Alloys Compd.*, 2021, **861**, 157974, DOI: **10.1016/j.jallcom.2020.157974**.
24 G. V. Manohara, M. M. Maroto-Valer and S. Garcia, *Dalton Trans.*, 2020, **49**, 923–931.
25 X. Tan, S. Liu, Y. Liu, Y. Gu, G. Zeng, X. Cai, Z. L. Yan, C. Yang, X. Hu and B. Chen, *Sci. Rep.*, 2016, **6**, 39691, DOI: **10.1038/srep39691**.
26 R. Soltani, A. Marjani and S. Shirazian, *Dalton Trans.*, 2020, **49**, 5323–5335.
27 J. Awassa, S. Soulé, D. Cornu, C. Ruby and S. El-Kirat-Chatel, *Nanoscale*, 2022, **14**, 10335–10348.
28 K. P. Hwang, H. C. Lin, Y. Z. Su, W. P. Wu and R. S. Yu, *J. Sol-Gel Sci. Technol.*, 2021, **97**, 441–451.
29 S. A. A. Abdel Aziz, Y. GadelHak, M. B. E. D. Mohamed and R. Mahmoud, *Sci. Rep.*, 2023, **13**, 7601, DOI: **10.1038/s41598-023-34488-y**.
30 P. K. Aspoukeh, A. A. Barzinjy and S. M. Hamad, *Int. Nano Lett.*, 2022, **12**, 153–168.
31 J. Wang, B. Wang, Z. Wang, L. Chen, C. Gao, B. Xu, Z. Jia and G. Wu, *J. Colloid Interface Sci.*, 2021, **586**, 479–490.
32 D. Y. Nadargi, M. S. Tamboli, S. S. Patil, I. S. Mulla and S. S. Suryavanshi, *SN Appl. Sci.*, 2019, **1**, 1564, DOI: **10.1007/s42452-019-1573-2**.
33 S. Das, A. Pal and A. Debnath, *ChemistrySelect*, 2023, **8**, e202300928, DOI: **10.1002/slct.202300928**.
34 A. Deb, S. Das and A. Debnath, *Chem. Phys. Lett.*, 2023, **830**, 140820, DOI: **10.1016/j.cplett.2023.140820**.
35 P. Zhou, J. An and X. Wen, *Mater. Res. Express*, 2019, **6**, 125529.
36 B. Saha, S. Shaji and A. Debnath, *J. Dispersion Sci. Technol.*, 2023, 2602–2616, DOI: **10.1080/01932691.2023.2273432**.
37 P. Das and A. Debnath, *J. Dispersion Sci. Technol.*, 2023, **44**, 2587–2598.
38 A. A. G. El-Shahawy, F. I. Abo El-Ela, N. A. Mohamed, Z. E. Eldine and W. M. A. El Rouby, *Mater. Sci. Eng., C*, 2018, **91**, 361–371.
39 I. Uddin, S. M. Abzal, K. Kalyan, S. Janga, A. Rath, R. Patel, D. K. Gupta, T. R. Ravindran, H. Ateeq, M. S. Khan and J. K. Dash, *ACS Omega*, 2022, **7**, 42438–42445.
40 I. Benchikh, F. Z. Dahou, S. Lahreche, L. Sabantina, Y. Benmimoun and A. Benyoucef, *Int. J. Environ. Anal. Chem.*, 2022, 4672–4691.
41 T. T. T. Nguyen, Y. N. N. Nguyen, X. T. Tran, T. T. T. Nguyen and T. Van Tran, *J. Environ. Chem. Eng.*, 2023, **11**, 111003, DOI: **10.1016/j.jece.2023.111003**.
42 H. M. Abo-Dief, S. M. El-Bahy, O. K. Hussein, Z. M. El-Bahy, M. Shahid and I. Shakir, *J. Alloys Compd.*, 2022, **913**, 165164.
43 L. Ma, Z. Chang, L. Guo, T. Li, G. Li and K. Wang, *Ionics*, 2020, **26**, 2537–2547.
44 B. A. Jiménez-López, R. Leyva-Ramos, J. J. Salazar-Rábago, A. Jacobo-Azuara and A. Aragón-Piña, *Environ. Nanotechnol., Monit. Manage.*, 2021, **16**, 100580.
45 L. Zhang, J. Liu, H. Xiao, D. Liu, Y. Qin, H. Wu, H. Li, N. Du and W. Hou, *Chem. Eng. J.*, 2014, **250**, 1–5.
46 B. Wiyantoko, P. Kurniawati, T. E. Purbaningtias, M. H. Jauhari, A. Yahya, M. Tamyiz, I. Fatimah and R. Doong, *Mater. Res. Express*, 2022, **9**, 035505.
47 X. Xiao, B. Peng, L. Cai, X. Zhang, S. Liu and Y. Wang, *Sci. Rep.*, 2018, **8**, 7571.
48 P. K. Samanta and A. K. Bandyopadhyay, *Appl. Nanosci.*, 2012, **2**, 111–117.
49 B. Tan, Y. Fang, Q. Chen, X. Ao and Y. Cao, *Opt. Mater.*, 2020, **109**, 110470, DOI: **10.1016/j.optmat.2020.110470**.
50 S. Majumder, N. D. Quang, N. M. Hung, N. D. Chinh, C. Kim and D. Kim, *J. Colloid Interface Sci.*, 2021, **599**, 453–466.
51 X. Wang, P. Wu, Z. Zhao, L. Sun, Q. Deng, Z. Yin and X. Chen, *J. Mater. Sci.: Mater. Electron.*, 2020, **31**, 4895–4904.

52 C. Jiehu, W. Chunlei, Z. Ming, Z. Jie, F. Li, D. Xiuhong, C. Leiming and L. Chunguang, *Appl. Surf. Sci.*, 2020, **534**, 147564.
53 T. V. M. Sreekanth, R. Ramaraghavulu, S. V. Prabhakar Vattikuti, J. Shim and K. Yoo, *Mater. Lett.*, 2019, **253**, 450–453.
54 S. K. Lakkaboyana, S. Khantong, N. K. Asmel, A. Yuzir and W. Z. Wan Yaacob, *J. Inorg. Organomet. Polym. Mater.*, 2019, **29**, 1658–1668.
55 C. Peng, J. Dai, J. Yu and J. Yin, *AIP Adv.*, 2015, **5**, 057138.
56 M. Daud, A. Hai, F. Banat, M. B. Wazir, M. Habib, G. Bharath and M. A. Al-Harthi, *J. Mol. Liq.*, 2019, **288**, 110989.
57 L. Santamaría, S. A. Korili and A. Gil, *Chem. Eng. J.*, 2023, **455**, 140551.
58 X. Wu, B. Li and X. Wen, *J. Nanopart. Res.*, 2017, **19**, 131, DOI: **10.1007/s11051-017-3803-0**.
59 M. Abbasi, M. M. Sabzehmeidani, M. Ghaedi, R. Jannesar and A. Shokrollahi, *J. Mol. Liq.*, 2021, **329**, 115558, DOI: **10.1016/j.molliq.2021.115558**.
60 M. Xie, X. Luo, C. Liu, S. You, S. Rad, H. He, Y. Huang and Z. Tu, *RSC Adv.*, 2022, **12**, 25833–25843.
61 Z. Zhang, D. Sun, G. Li, B. Zhang, B. Zhang, S. Qiu, Y. Li and T. Wu, *Colloids Surf., A*, 2019, **565**, 143–153.
62 B. Saha, A. Debnath and B. Saha, *Mater. Today Commun.*, 2024, **39**, 109061, DOI: **10.1016/j.mtcomm.2024.109061**.
63 R. A. Hakro, M. Mehdi, R. F. Qureshi, R. B. Mahar, M. Khatri, F. Ahmed, Z. Khatri and I. S. Kim, *Mater. Res. Express*, 2021, **8**, 055502.
64 F. Mashkoor, A. Nasar, Inamuddin and A. M. Asiri, *Sci. Rep.*, 2018, **8**, 8314.
65 Y. Li, H. Lu, Y. Wang, Y. Zhao and X. Li, *J. Mater. Sci.*, 2019, **54**, 7603–7616.
66 F. C. Wu, R. L. Tseng and R. S. Juang, *Chem. Eng. J.*, 2009, **153**, 1–8.
67 S. Das, S. Rudra Paul and A. Debnath, *J. Mol. Liq.*, 2023, **387**, 122610, DOI: **10.1016/j.molliq.2023.122610**.
68 N. T. K. Phuong, M. Beak, B. T. Huy and Y.-I. Lee, *Chemosphere*, 2016, **146**, 51–59.
69 R. Shabbir, A. Gu, J. Chen, M. M. Khan, P. Wang, Y. Jiao, Z. Zhang, Y. Liu and Y. Yang, *Int. J. Environ. Anal. Chem.*, 2022, **102**, 1060–1077.
70 I. E. Medina-Ramírez, C. E. D. de León-Macias, G. Pedroza-Herrera, R. Gonzáles-Segovia, J. A. Zapien and J. L. Rodríguez-López, *Ceram. Int.*, 2020, **46**, 8979–8994.
71 L. Pan, Q. Zhu and D. Tian, *J. Sol-Gel Sci. Technol.*, 2019, **90**, 525–534.
72 Y. W. Wang, A. Cao, Y. Jiang, X. Zhang, J. H. Liu, Y. Liu and H. Wang, *ACS Appl. Mater. Interfaces*, 2014, **6**, 2791–2798.